Mixing Matrix Calibration for BSS Range Ambiguity Suppression in Multichannel SAR Systems

Ershad Junus Amin, Gerhard Krieger, *Fellow, IEEE*, Marwan Younis, *Fellow, IEEE*, Federica Bordoni, and Alberto Moreira, *Fellow, IEEE*

***Abstract*— A significant level of range ambiguity disturbance may affect high-resolution wide-swath spaceborne synthetic aperture radar (SAR) systems with multiple elevation receive beams. To overcome this limitation, a promising approach, based on the higher order blind source separation (BSS), was recently proposed. This method, denoted as range ambiguity BSS (RABSS), demonstrates outstanding range ambiguity suppression performance when applied to heterogeneous scenes. Nevertheless, a degradation is expected for relatively homogeneous scenes. In this letter, the RABSS method is extended by introducing a novel mixing matrix calibration procedure. The robustness of the proposed approach towards different types of imaged surfaces is numerically analyzed by means of realistic simulations, which rely on the backscattering coefficients of TerraSAR-X images and the simulated antenna patterns of a large array-fed reflector antenna employing multiple elevation beams.**

***Index Terms*— Blind source separation (BSS), digital beamforming (DBF), high-resolution wide-swath, synthetic aperture radar (SAR).**

I. Introduction

MULTICHANNEL spaceborne synthetic aperture radar (SAR) systems with digital beamforming (DBF) capability have been intensively studied and developed in the last decades, to overcome the trade-off between swath extension and spatial resolution of conventional SAR systems. Outstanding examples of these high-resolution wide-swath (HRWS) SAR systems are the U.S.-Indian NISAR mission, scheduled for launch in 2024, and the German mission proposal Tandem-L (TDL) [1], [2]. Both systems employ an array-fed reflector antenna to implement a multi-beam operational mode: on transmission (Tx), a broad beam illuminates a wide swath, at high pulse repetition frequency (PRF); on receive (Rx), multiple narrow elevation beams, each operating according to the scan-on-receive (SCORE) DBF technique, collect the useful signals [3].

A considerable challenge of a multi-beam operational mode is the suppression of range ambiguities (Fig. 1). In fact, the signal that is useful for one Rx beam represents a range ambiguity for another beam. Accordingly, the range ambiguities cannot be attenuated by the transmit antenna patterns, as in a conventional case, and may reach a significant level. In principle, an accurate knowledge of the antenna pattern would allow to suppress the ambiguities. The optimum ambiguity suppression is, however, difficult to achieve in practice, as an accurate measurement of the antenna patterns on ground is not always feasible, especially for large reflector antennas; deformations and thermal instabilities can significantly alter the shape of the nominal antenna pattern and errors associated with the Tx and Rx channels, mispointing, and inaccurate topographic height may degrade the pattern estimation accuracy [4], [5].

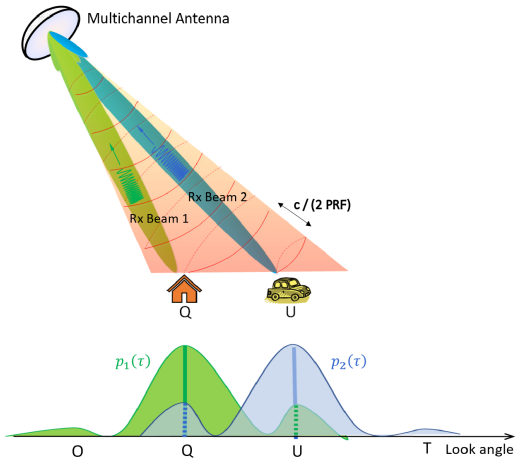

Fig. 1. Zero-Doppler geometry. Two subswaths are imaged simultaneously using a wide Tx beam and two narrow Rx beams, where $c/(2\ \mathrm{PRF})$ is the range ambiguity distance, c the speed of light.

In [6], for the first time, the issue of range ambiguity suppression in SAR systems with multiple elevation beams is formulated as a cocktail party problem. Specifically, the antenna pattern estimation is expressed as a mixing matrix (MM) estimation, and a solution based on the blind source separation (BSS) technique is proposed. Starting from this first work, a novel data-based method relying on the higher order (HO) BSS, denoted here as range ambiguity BSS (RABSS), was presented and analyzed in detail in [7].

A remarkable aspect of RABSS is that it does not require any prior knowledge of the actual antenna pattern, i.e., it estimates the MM directly from the acquired SAR data. Additionally, it does not affect the SAR instrument complexity, since it is applied on-ground to the downlinked data.

The RABSS method demonstrates very good performance. Nevertheless, its effectiveness over homogeneously backscattering scenes remains uncertain, since the HO BSS technique performs optimally when the signals to be retrieved have

Manuscript received 15 November 2023; revised 21 December 2023 and 13 February 2024; accepted 28 February 2024. Date of publication 1 March 2024; date of current version 15 March 2024. *(Corresponding author: Ershad Junus Amin.)*

The authors are with the Microwaves and Radar Institute, German Aerospace Center, 82234 Weßling, Germany (e-mail: Ershad.Amin@dlr.de).

Digital Object Identifier 10.1109/LGRS.2024.3372654

non-Gaussian statistics [8]. To increase the robustness of the RABSS method towards homogeneous imaged scenes, a novel approach, denoted as calibrated-RABSS (C-RABSS), is presented in this letter. Specifically, to effectively handle various types of scenes, a MM calibration procedure is incorporated in the HO BSS.

The letter is structured as follows. Section II recalls the RABSS method and the problem formulation; Section III presents the proposed C-RABSS method; Section IV analyzes and validates C-RABSS numerically; Section V concludes the letter.

II. Problem Statement

Let us refer, without loss of generality, to the simple scenario in Fig. 1: an HRWS SAR system illuminates the overall imaged swath, at high PRF, by means of a wide Tx beam; on Rx, $N = 2$ narrow elevation beams are used to simultaneously collect the radar echos from N subswaths according to the SCORE technique [1], [2], [3]. The imaged surface shows four point targets (O, Q, U, and T), separated by the range ambiguity distance: Q and U are located in the first and second imaged subswath, respectively; O and T outside the imaged swath. Accordingly, in the first beam, Q returns the useful signal, and U the strong range ambiguity; in the second beam, U returns the useful signal, and Q the strong range ambiguity; O and T are weak ambiguities that are already attenuated by the Tx pattern. In this scenario, the instantaneous Rx signal can be expressed as follows [6], [7], [9]:

$$\begin{aligned}\mathbf{x}(\tau, f_t) &= \mathbf{A}(\tau, f_t) \cdot \mathbf{s}(\tau, f_t) + \mathbf{s}_{\mathrm{WA}}(\tau, f_t) + \mathbf{n} \\ \begin{bmatrix} x_1(\tau, f_t) \\ x_2(\tau, f_t) \end{bmatrix} &= \begin{bmatrix} 1 & a_{12}(\tau, f_t) \\ a_{21}(\tau, f_t) & 1 \end{bmatrix} \cdot \begin{bmatrix} \mathbf{s}_1(\tau, f_t) \\ \mathbf{s}_2(\tau, f_t) \end{bmatrix} \\ &\quad + \begin{bmatrix} s_{1,\mathrm{WA}}(\tau, f_t) \\ s_{2,\mathrm{WA}}(\tau, f_t) \end{bmatrix} + \begin{bmatrix} n_1 \\ n_2 \end{bmatrix} \end{aligned} \tag{1}$$

where τ and f_t denote the range time and the azimuth frequency, respectively; $\mathbf{s}$ is the useful signal; $\mathbf{s}_{\mathrm{WA}}$ is the weak ambiguity signal; $\mathbf{n}$ is the additive noise; $\mathbf{A}$ is the MM, with antidiagonal elements given by

$$a_{12}(\tau, f_t) = \frac{p_1(\tau, f_t, \mathrm{U})}{p_2(\tau, f_t, \mathrm{U})}, \quad a_{21}(\tau, f_t) = \frac{p_2(\tau, f_t, \mathrm{Q})}{p_1(\tau, f_t, \mathrm{Q})} \tag{2}$$

where p_j denotes the two-way antenna pattern, used to image the jth subswath ($j = 1, 2$), evaluated at the position of U or Q.

From (1) and (2), the useful signal can be estimated as

$$\hat{\mathbf{s}} = \hat{\mathbf{B}}\mathbf{x} \tag{3}$$

where $\hat{\mathbf{B}}$ denotes a proper estimate of the separation matrix, the actual separation matrix is $\mathbf{B} \approx \mathbf{A}^{-1}$, and the approximation is due to the presence of the weak ambiguities and the additive noise [6], [7].

From (1)–(3), it is clear that an accurate estimate of the useful signal is equivalent to an effective suppression of the range ambiguities. Furthermore, the reported mathematical model highlights the relevance of the MM, $\mathbf{A}$, or equivalently of the antenna pattern: any inaccuracies in the estimation of the MM may result in an incorrect retrieval of the useful signal, leading to a suboptimal range ambiguity suppression.

The problem of estimating the useful SAR signal is similar to the cocktail party problem [6], [7], [9]. To solve this "SAR cocktail party problem," an approach based on a HO BSS technique, here denoted as RABSS method, was proposed and analyzed in [7]. The choice of such a HO approach in the SAR context is justified by the statistical independence between the useful signals[1] [8], [10]. In fact, the idea behind the HO BSS techniques comes from the central limit Theorem [11], which states that the sum of an infinitely large number of independent random variables will result in a Gaussian random variable. Moreover, the selection of the HO approach is motivated by its robustness against noise [12].

In [7], it was shown that the RABSS method has the capability to improve the range ambiguity suppression by up to −16 dB for heterogeneous scenes. Nevertheless, the HO BSS relies on the assumption that the Rx signals exhibit non-Gaussian characteristics [8]. It is then reasonable to expect that the RABSS achievable performance depends on the imaged backscattering surface and the statistics of the Rx signal [7]. In particular, an increasing level of homogeneity in the backscattering surfaces, or equivalently an increasing Gaussianity of the Rx signal, may be critical [7], [13].

III. Calibrated RABSS Method

The proposed novel method, denoted as C-RABSS, relies on the evaluation of the effectiveness of RABSS in different acquisition scenarios, based on the Gaussianity of the Rx signals. In particular, in accordance with the properties of the HO BSS technique [8], it assumed that the RABSS method achieves better performance if no more than one of the simultaneously received signals is Gaussian. In fact, in this case, all the Rx signals can be distinguished and individually estimated by the HO BSS. Conversely, when multiple Rx signals are Gaussian, the HO BSS allows to estimate the non-Gaussian signals, but cannot separate the Gaussian signals based on their HO statistical properties.[2]

To numerically quantify the RABSS effectiveness, a separation index is defined. Specifically, the separation index is derived from the kurtosis of the N Rx data matrices, that are considered as input of the HO BSS processing step in the RABSS method, as follows:

$$s_{\mathrm{idx}} = \mathrm{floor}\left\{ \frac{\sum_{i=1}^{M} f(i)}{M} \times 10 \right\} \tag{4}$$

where floor{·} denotes the floor operator (lower integer associated with a floating number); M denotes the total number of range samples, collected by each of the N Rx data matrices from the corresponding imaged subswath; the function $f(i)$ of the ith range sample is given by

$$f(i) = \begin{cases} 1, & \text{if } Y_i \geq N - 1 \\ 0, & \text{otherwise} \end{cases} \tag{5}$$

[1]The useful signals are expected to be mutual independent, since they are spatially separated by the distance of ambiguity.

[2]Since $\mathbf{s}$ is a priori not known, this condition is here applied, by means of (5) and (6) to the Rx signals, $\mathbf{x}$, which are anyway expected to have a comparable Gaussianity.

where $1 \leq i \leq M$, and

$$Y_i = \sum_{j=1}^{N} \left[|\mathrm{CSK}(x_j(i))| > 2.3 \right] \tag{6}$$

$x_j(i)$ denoting an azimuth line of the jth Rx data matrix for each of the N imaged subswath, CSK is the complex signal kurtosis [13], and 2.3 being the assumed threshold value for a Gaussian distribution based on empirical evaluation (i.e., a Gaussian distribution is assumed to occur when the measured CSK value falls within the range of −2.3 to 2.3).

From (4)–(6), it can be seen that s_{idx} is an integer number ranging from 0 to 10, obtained by averaging over M range samples: the closer the value to 10, the lower the Gaussianity of the received signal, and the homogeneity of the imaged scene, i.e., the better the expected RABSS performance in terms of estimation of the MM.

The computed separation index value, s_{idx}, is used then in the C-RABSS method to refine the estimation of the MM, i.e., to calibrate the MM, based on the heterogeneity of the currently imaged scene. Specifically, when s_{idx} is higher than a proper threshold value, k, a significant heterogeneity is assumed and the basic RABSS procedure is employed to obtain the estimated separation matrix, $\hat{\mathbf{B}}$. Conversely, when s_{idx} does not exceed k, a relatively homogeneity is assumed and a different approach is adopted: instead of applying the HO BSS directly to the actual Rx signals, $\hat{\mathbf{B}}$ is borrowed from a previously acquisition scene with a $s_{\mathrm{idx}} > k$. In fact, as shown in (1) and (2), the MM, $\mathbf{A}$, (and consequently in first approximation the separation matrix, $\mathbf{B}$) depends on the antenna pattern and the acquisition geometry, but is independent on the kind of backscattering surface; only the estimation of the MM depends on the backscatter through the HO BSS performance. Accordingly, it is expected to be advantageous to use a MM estimation, obtained from a strongly heterogenous scene rather than from a relatively homogeneous scene. Note that in presence of a $s_{\mathrm{idx}} > k$, the MM is computed based on the actual acquisition scenario, even if a MM estimation with a higher s_{idx} may be available. This is done to properly account for the actual antenna pattern shape, which may be influenced by the temperature or pointing variations. For the selection of the threshold value, k, both the Gaussianity level and the system architecture are considered. In fact, for a given imaged scene, the BSS capability to estimate the MM is influenced by the basic structure of the matrix (mean level of the antidiagonal elements), determined by the system architecture [7]. Specifically, an empirical analysis, based on the knowledge of the nominal patterns, is implemented, as explained more in detail in Section IV (see Fig. 4).

As regards the complexity of the C-RABSS method, it is worth to remark that C-RABSS is not supposed to be repetitively applied over short acquisition intervals, but is a periodic calibration tool. In fact, the MM can be assumed to be stable during a few consecutive acquisitions. Moreover, sufficiently long data takes (data samples) are required by RABSS to accurately estimate the MM.

TABLE I
REFERENCE SYSTEM PARAMETERS

Parameter	Value
Orbit height	628 km
No. channels in elevation	35
Elevation tilt angle w.r.t. nadir	36 deg
Center frequency	1.26 GHz
PRF	2700 Hz
Chirp bandwidth	38 MHz
Processed Doppler bandwidth	1348 Hz
Pulse duration	30 μs
Signal-to-noise ratio	10 dB

IV. NUMERICAL ANALYSIS

A reference DBF HRWS SAR system, based on an array-fed reflector antenna, is here considered. Its key parameters are provided in Table I. The system implements a multibeam operational mode: a broad Tx beam, obtained by activating simultaneously all the feeds elements, illuminates a swath on the ground of approximately 300 km; a pulse repetition frequency (PRF) of 2700 Hz is chosen to achieve an azimuth resolution of 6 m; five narrow SCORE Rx beams, formed by activating consecutive sets of feed elements, simultaneously collect the echo from five mutually range-ambiguous subswaths. Accordingly, during the imaging process, the system receives four strong ambiguous echoes. Moreover, two weak ambiguities are considered, originating from the near and far range, respectively.

To assess the C-RABSS robustness against various types of backscattering surfaces, nine SAR data are simulated, each characterized by a different degree of scene homogeneity. The corresponding SAR focused images are shown in Fig. 2. To ensure the realism of the simulation, the data are generated using the Tandem-L (TDL) antenna patterns [1] and the actual backscattering coefficient of real SAR images, acquired by TerraSAR-X (TSX) [14].

Fig. 3 shows a comparison between the actual MM and the MM estimation, derived from the RABSS method in [7], for two different scenes: (a) the heterogeneous scene in Fig. 2(5); and (b) the homogeneous scene in Fig. 2(1). The degradation of the RABSS estimation performance for the homogeneous scene is evident.

Fig. 4 shows the MM correlation coefficient (MMCC) versus the separation index, s_{idx}, for the nine different acquisition scenes in Fig. 2. Here, the MMCC quantifies the RABSS capability to properly estimate the MM. In fact, it measures the similarity between the actual MM and the MM estimation, obtained by the RABSS (0 indicates no correlation, 1 full correlation). For instance, the obtained MMCC value is 0.85 for the heterogeneous scene in Fig. 2(5), and 0.17 for the homogeneous scene in Fig. 2(1). The comparison between the MMCC and s_{idx} confirms the expected degradation of the RABSS estimation performance for homogeneous scenes, such as the scene depicted in Fig. 2(6), and the improving performance for heterogeneous scenes, such as the scene depicted in Fig. 2(5). Fig. 4 also serves as a tool for empirically select the threshold, k, for s_{idx} for the considered system architecture. Specifically, a value of $k = 8$, is selected as the

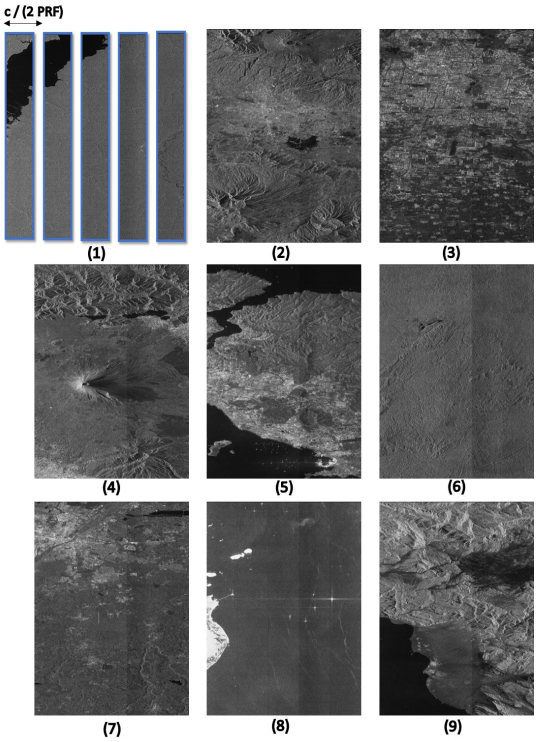

Fig. 2. Simulated focused SAR images, derived from a real TSX complex SAR image [14]. Each image is composed of five range-ambiguous subswaths,[3] as highlighted in the scene (1). The horizontal axis represents the range direction and the vertical axis the azimuth direction.

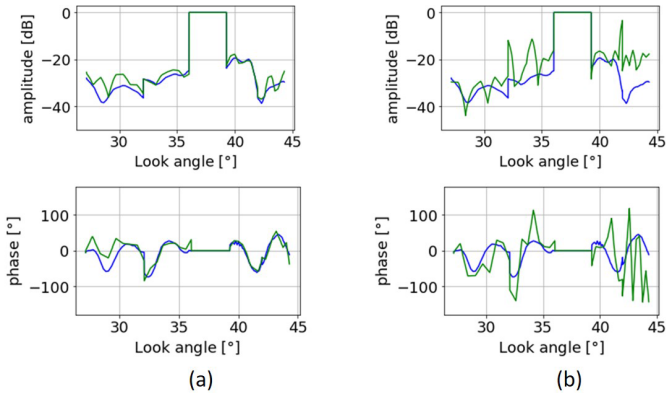

Fig. 3. Amplitude (top) and phase (bottom) of the actual (blue curve) and estimated MM (green curve), obtained by the RABSS method [7], versus off-nadir angle. Two SAR acquisition scenes are considered: (a) heterogeneous scene in Fig. 2(5); (b) homogeneous scene in Fig. 2(1). The spatial separation between the subswaths is here not visualized.

threshold in the proposed C-RABSS method, to indicate an accurate estimation of the RABSS MM. Furthermore, $s_{\text{idx}} > 8$ is obtained for the heterogeneous scenes in Fig. 2(5) and (3).

Fig. 5 shows a comparison between the range ambiguity-to-signal ratio (RASR) performance, obtained by the RABSS and the proposed C-RABSS method, for the nine acquisition scenes in Fig. 2. As a benchmark, also the initial RASR, i.e., the RASR measured on the simulated SAR data without the application of any method, is reported. For the scene (3) and (5), the RABSS and C-RABSS methods obviously show the same performance; in the other cases the C-RABSS method achieves a RASR improvement up to 18 dB (on average 6 dB) compared to the initial one, and outperforms the RABSS. The advantage of C-RABSS is particularly relevant for the strong homogeneous scenes (1) and (6), where the RABSS method completely fails, achieving a RASR significantly

[3]Each subswath is simulated and processed individually. In fact, there is no continuity between subswaths due to the limited number of simulated samples. Therefore, a brightness gap is visible, for instance, in the middle-right of the image.

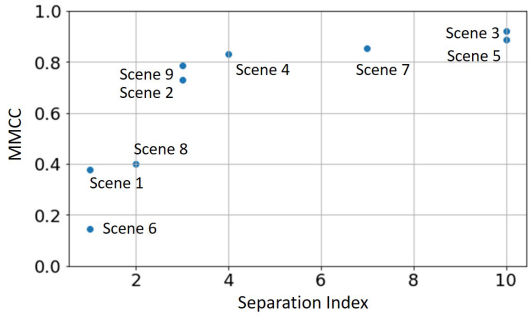

Fig. 4. MMCC versus separation index, for the nine scenes in Fig. 2.

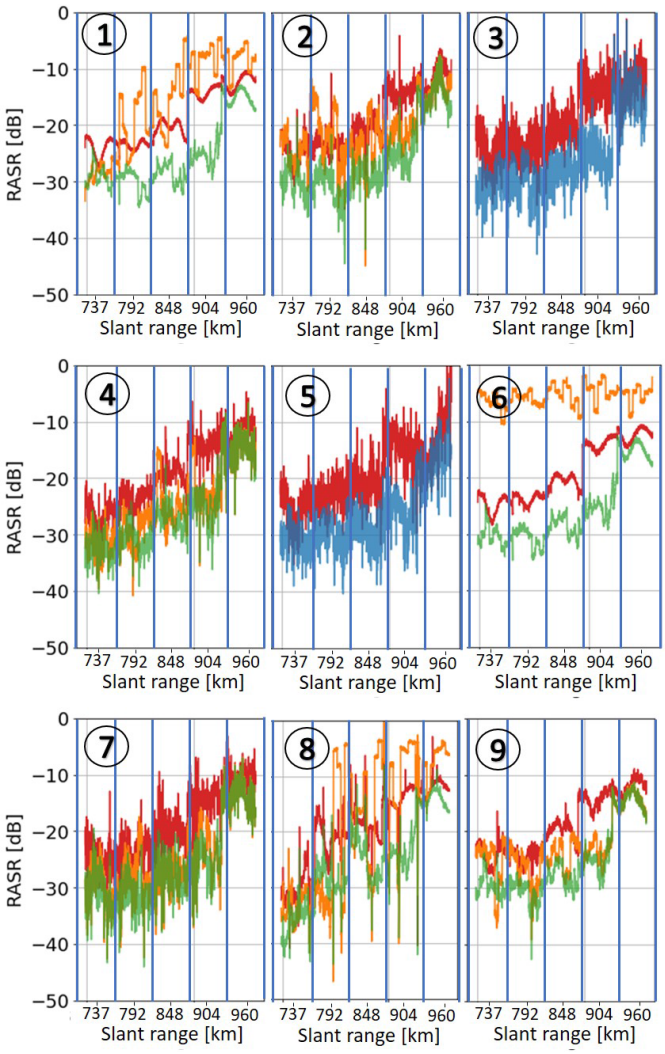

Fig. 5. RASR performance for the nine scenes in Fig. 2: RABSS (orange); C-RABSS (green); initial (red). The blue curve in scenes 3 and 5 denotes the performance of RABSS and C-RABSS, which are the same. The blue vertical lines indicate the boundary between the simulated swath segments. The circled number refers to the scene.

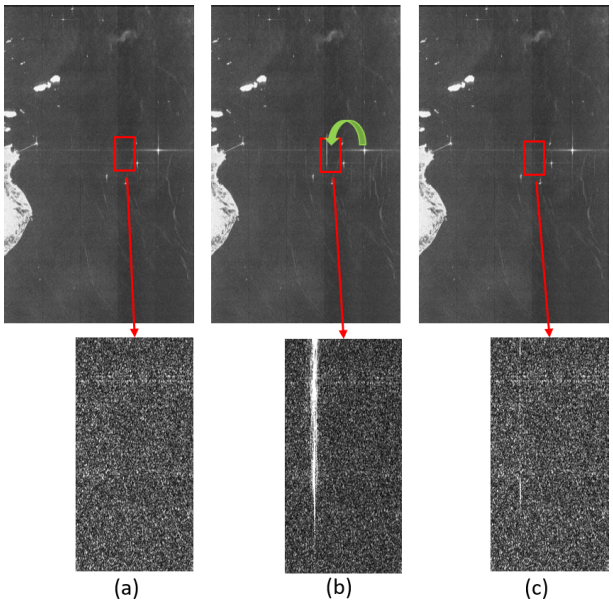

Fig. 6. Simulated and focused SAR images for the scene in Fig. 2(8): (a) ambiguity-free image; (b) initial ambiguous image; (c) ambiguity-suppressed image by the proposed C-RABSS method. The closer view is depicted in the bottom figure, where the range ambiguity is suppressed by 18 dB. The horizontal axis indicates the range direction, the vertical axis the azimuth. The spatial separation between the simulated swath segments is here not visualized.

poorer than the initial one. Nevertheless, the limited improvement in the far range is attributed to the presence of weak ambiguity signals, which is also an issue in the RABSS method. Moreover, Fig. 5(8), around the 792 km slant range, shows that the C-RABSS performance may be challenging in specific scenarios characterized by very strong variations of the backscattering level. The investigation of such an effect goes anyway beyond the aim of the present work and is remanded to future analysis.

Finally, to provide a qualitative assessment of the achieved ambiguity suppression, Fig. 6 shows three simulated, focused, SAR images. They all refer to the scene in Fig. 2(8): (a) the ambiguity-free image; (b) the initial, ambiguous, image; and (c) the ambiguity-suppressed image, obtained using the proposed C-RABSS method. The closer examination of the areas indicated by red boxes highlights the presence of a significant ambiguity in Fig. 6(b). The displayed range ambiguity disturbance originates from a strong backscattering point-like target, located outside the red box on the right as indicated by the green arrow. Clearly recognizable for this ambiguity is the smearing in the azimuth direction due to the mismatched azimuth compression. Nevertheless, the C-RABSS demonstrates the effectiveness of the proposed method for suppressing range ambiguity.

V. Conclusion

A new range ambiguity suppression method for advanced multichannel spaceborne SAR systems with multiple elevation receive beams is presented. The method, denoted as C-RABSS, is obtained from the recently proposed range ambiguity suppression method based on the HO BSS technique (RABSS). Specifically, the C-RABSS method includes a novel MM calibration procedure to improve the RABSS robustness against relatively homogeneous imaged scenes. The rationale of the C-RABSS method is explained in detail. The performance of the C-RABSS method and that of the RABSS are numerically investigated in realistic simulation scenarios. These are generated using the antenna patterns from Tandem-L and the backscattering coefficients of real TerraSAR-X images, representing scenes with different homogeneity level. The obtained results show that C-RABSS can achieve a maximum range ambiguity suppression of 18 dB, with an average suppression of 6 dB for various surface types, clearly demonstrating the superiority of C-RABSS, compared to the RABSS method, and its effectiveness in suppressing range ambiguities independently of the specific, homogeneous or heterogeneous, backscatter of the imaged scene.

References

[1] S. Huber, F. Q. de Almeida, M. Villano, M. Younis, G. Krieger, and A. Moreira, "Tandem-L: A technical perspective on future spaceborne SAR sensors for Earth observation," *IEEE Trans. Geosci. Remote Sens.*, vol. 56, no. 8, pp. 4792–4807, Aug. 2018.

[2] K. Kellogg et al., "NASA-ISRO synthetic aperture radar (NISAR) mission," in *Proc. IEEE Aerosp. Conf.*, Mar. 2020, pp. 1–21.

[3] M. Suess, B. Grafmueller, and R. Zahn, "A novel high resolution, wide swath SAR system," in *Proc. Scanning Present Resolving Future. IEEE Int. Geosci. Remote Sens. Symp.*, Jul. 2001, pp. 1013–1015.

[4] S. Huber, M. Younis, G. Krieger, and A. Moreira, "Error analysis for digital beamforming synthetic aperture radars: A comparison of phased array and array-fed reflector systems," *IEEE Trans. Geosci. Remote Sens.*, vol. 59, no. 8, pp. 6314–6322, Aug. 2021.

[5] K. Mouthaan, "Digital beamforming for spaceborne reflector SAR systems via fir filter networks in the presence of uncertainties," Ph.D. dissertation, Institut für Luft- und Raumfahrt (ILR), TU Berlin, Berlin, Germany, 2017.

[6] G. Krieger et al., "CEBRAS: Cross elevation beam range ambiguity suppression for high-resolution wide-swath and MIMO-SAR imaging," in *Proc. IEEE Int. Geosci. Remote Sens. Symp. (IGARSS)*, Jul. 2015, pp. 196–199.

[7] E. J. Amin, G. Krieger, M. Younis, F. Bordoni, A. B. C. da Silva, and A. Moreira, "A 2-D range ambiguity suppression method based on blind source separation for multichannel SAR systems," *IEEE Trans. Geosci. Remote Sens.*, vol. 62, 2024, Art. no. 5203117.

[8] A. Hyvärinen and E. Oja, "Independent component analysis: Algorithms and applications," *Neural Netw.*, vol. 13, nos. 4–5, pp. 411–430, Jun. 2000.

[9] E. Amin, M. Younis, and G. Krieger, "Two-dimensional range ambiguity suppression in multichannel SAR using blind source separation method," in *Proc. EUSAR 13th Eur. Conf. Synth. Aperture Radar*, Mar. 2021, pp. 1–5.

[10] J. F. Cardoso and A. Souloumiac, "Blind beamforming for non-Gaussian signals," *IEE Proc. F Radar Signal Process.*, vol. 140, no. 6, p. 362, 1993.

[11] A. Papoulis, *Probability and Statistics*. Upper Saddle River, NJ, USA: Prentice-Hall, 1990.

[12] M. H. Fatnan, Z. M. Hussain, and H. R. Mohammed, "Blind source separation under semi-white Gaussian noise and uniform noise: Performance analysis of ICA, sobi and JadeR," *J. Comput. Sci.*, vol. 15, no. 1, pp. 27–44, Jan. 2019.

[13] X. Leng, K. Ji, S. Zhou, and X. Xing, "Ship detection based on complex signal kurtosis in single-channel SAR imagery," *IEEE Trans. Geosci. Remote Sens.*, vol. 57, no. 9, pp. 6447–6461, Sep. 2019.

[14] G. Krieger et al., "TanDEM-X: A satellite formation for high-resolution SAR interferometry," *IEEE Trans. Geosci. Remote Sens.*, vol. 45, no. 11, pp. 3317–3341, Nov. 2007.